Paper No.
C2025-00326

AMPP ANNUAL CONFERENCE + EXPO
APRIL 6-10, 2025 | NASHVILLE, TENNESSEE

Formation of Iron Sulfides at Elevated Temperature (80-160 °C) and their Effect on Corrosion of Mild Steel

Zhuldyz Zhigulina, Bruce Brown, David Young, Marc Singer
Institute for Corrosion and Multiphase Technology
Department of Chemical and Biomolecular Engineering
Ohio University
Athens, OH 45701
USA

ABSTRACT

Both H_2S and CO_2, ubiquitous in hydrocarbon production and processing, have the potential to severely compromise asset integrity. While both are corrosive, H_2S containing environments can be particularly aggressive, causing more rapid and severe corrosion compared to CO_2; especially in high temperature oil and gas production systems. There has been limited investigation of H_2S corrosion at elevated temperatures, resulting in a deficient understanding of the underlying mechanisms responsible for observed phenomena. Consequently, corrosion research related to the presence of H_2S gas is of particular interest to the oil and gas industry. The key goal of the experimental work herein was to compare observed phenomena for high temperature H_2S corrosion against results from previous investigations, with a deepened data analysis. Data for autoclave experiments conducted at $pH_{initial}$ 4.0, 0.00385M $[H_2S]_{aq}$ (1.6-2.0% H_2S) contrasting corrosion product layers at 80 and 160 °C are reported. Experimental results using two API 5L X65 mild steels demonstrate that corrosion rates at 80 and 160 °C were essentially the same, within measurement error, with mackinawite found at 80 °C and a combination of iron sulfides (pyrrhotite, mackinawite) with magnetite found at 160 °C. However, localized corrosion appeared on the X65 specimens at 160 °C.

Keywords: H_2S, CO_2, iron sulfide, high temperature

INTRODUCTION

The oil and gas industry is strongly dependent on the integrity of steel tubulars used for extraction and transmission of hydrocarbons. As a result, research associated with the potential deterioration of steel assets in contact with produced fluids, which often contain highly corrosive gases such as CO_2 and H_2S, is of essential importance. Sour (associated with the presence of H_2S) and sweet (associated with CO_2 only) corrosion of carbon steel involves interrelated processes; each has been the topic of intense research over the last 70 years. While sweet corrosion is relatively well understood, this is not the case for sour corrosion.[1] This is due to the complexity of the corrosion mechanisms in the presence of H_2S.[2] Although the history of H_2S corrosion research goes back to the 1940s, there are many contradictions related to proposed mechanisms of corrosion and corrosion product formation.[3] One of the first literature on corrosion products in H_2S environments is the study of Shoesmith, *et al*., at pH of 4.0.[4] They postulated that mackinawite, which initially forms on the surface of steel, gradually converts to cubic FeS and some troilite, which becomes the dominant corrosion products after 96 hours.

Bai, *et al*., also discussed the effect of time on the change in the corrosion product layer at 50 °C with 10 bar pH_2S.[5] The main corrosion products observed after 6 and 12 hours of exposure were mackinawite and cubic FeS. Then, these layers transformed into troilite, making it the main corrosion product after 96 hours of exposure to this environment; note that all three of these phases are crystallographically distinct FeS polymorphs. The conclusions were similar to Shoesmith, *et al*.[4], however, key information such as pH was missing in this work.

Ning, *et al*., conducted experiments on steel specimens exposed to 0.097 bar pH_2S, pH 6.0, and 25 °C for 4 days, observing that a poorly protective and porous mackinawite (FeS) corrosion product layer formed on the surface.[6] At the same conditions but higher temperature of 80 °C, a more dense, adherent and consequently more protective layer comprised of a mixture of mackinawite (FeS) and pyrrhotite ($Fe_{1-x}S$) was identified.

Studies on the mechanisms related to H_2S corrosion at high temperatures have rarely been published, mainly due to the complexity and safety considerations associated with high temperature experimentation using such a toxic gas. Nevertheless, different theories have been proposed to explain corrosion product formation mechanisms in a sour system at elevated temperatures. In upstream oil and gas industry applications, high temperatures typically mean a range between 80 and 200 °C – this is the focus of the present research.

Gao conducted a series of experiments in H_2S environments at elevated temperatures of 80-200 °C, pH 4.0, and 0.10-0.18 bar pH_2S, using N_2 as the balance gas.[1] Different iron sulfide polymorphs and related phases were formed based on the temperature the steel was exposed to: mackinawite at 80 °C, troilite at 120 °C, pyrrhotite ($Fe_{1-x}S$) at 160 °C, and a mixture of pyrrhotite and pyrite (FeS_2) at 200 °C. The presence of pyrite was associated with occurrence of localized corrosion on the API X65 mild steel specimens used. Through analysis of cross-sections of the mild steel specimens, he also observed that there was an inner layer of iron oxide underneath the iron sulfide and proposed a mechanism to explain his experimental observations. As Fe starts dissolving under the influence of this corrosive environment, Gao concluded that the released Fe^{2+} ions first react to form an oxide:

$$3Fe^{2+}_{(aq)} + 4H_2O_{(l)} \leftrightarrow Fe_3O_{4\,(s)} + 8H^+_{(aq)} + 2e^- \qquad (1)$$

As the reaction proceeds, the layer of Fe_3O_4 forms, followed by the diffusion of H_2S to the Fe_3O_4/FeS interface. Then, H_2S reacts with Fe_3O_4, which, as a result, contributes to the growth of the FeS layer:

$$Fe_3O_{4\,(s)} + 3H_2S_{\,(aq)} + 2H^+_{(aq)} + 2e^- \leftrightarrow 3FeS_{(s)} + 4H_2O_{(l)} \quad (2)$$

The rate of this reaction increases until the Fe_3O_4 reaction achieves a steady state. The iron sulfide layer continues to grow at the FeS/solution interface when the saturation value of FeS in the bulk is above the solubility limit of iron sulfide.[7]

In this study, the observed phenomena related to high-temperature H_2S corrosion of mild steel are compared with results from Gao's previous investigations conducted in our laboratory, along with a more detailed data analysis. Conducting this study using a mechanistic approach is essential for verifying alignment with previous findings, thereby establishing reliability in the literature and the current research. It is crucial for building confidence in the experimental methodology before progressing to more complex systems involving both H_2S and CO_2 gases.

EXPERIMENTAL APPARATUS AND PROCEDURE

The experimental setup for high temperature corrosion measurements is shown schematically in Figure 1. The 7.5 liter autoclave contains a three electrode system using a platinum coated niobium counter electrode (CE), an API 5L X65 carbon steel working electrode (WE), and a Ag/AgCl refillable reference electrode (RE) for high temperatures and high pressures systems purchased from Corr Instruments†.

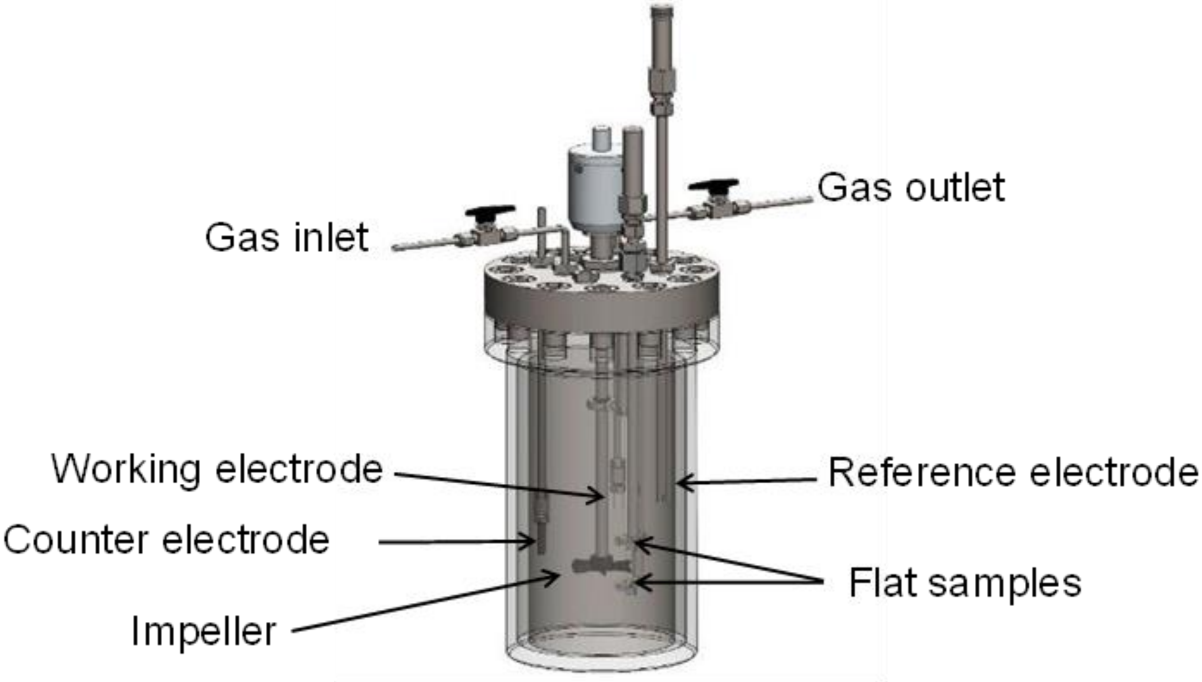

Figure 1. Experimental 7.5-liter autoclave setup with parts labeled

Due to the unavailability of a reliable pH electrode for high temperature measurements in an H_2S environment, a procedure was implemented to calculate the pH during the high temperature phase of each experiment using a water chemistry model; a similar procedure was used by Gao. The pH of the N_2 sparged solution was measured

---

† Trade name

with an Omega[‡] PHE-5431-10 pH probe and was adjusted based on water chemistry calculations at 50 °C, to achieve pH 4.0 at either 80 or 160 °C after the addition and equilibration of H_2S.

Two different types of API 5L X65 (referred to as “X65”) steel were used in experiments conducted at 160 °C; the compositions of these materials are shown in Table 1, with the primary difference being their carbon content. Previous tests conducted by Gao[1] used X65-0.13%C, while later testing was performed using a X65-0.05%C material. These tests aimed to assess whether the differences in composition influenced the experimental results. The experimental conditions are outlined in Table 2.

Table 1
Percent composition of API 5L X65 low alloy steels

	Material	**C**	**Cr**	**Mo**	**Cu**	**V**	**Si**	**Al**	**Ni**	**Mn**	**Fe**
WE**,** Two flat samples	X65-0.05%C	0.05	0.23	0.07	0.11	0.03	0.22	0.02	0.24	1.40	Bal
Two flat samples	X65-0.13%C	0.13	0.14	0.16	-	0.047	0.26	-	0.36	1.16	Bal

(information not given in analysis is noted by “-“)

Table 2
Test Matrix

Parameter	**Conditions**	
System	7.5-Liter autoclave	
Solution	1 wt.% NaCl	
Temperature, °C	80	160
Material	X65-0.05%C: WE (A_s=5.36 cm^2), and 2 flat specimens (A_s=6.4 cm^2 each)	X65-0.05%C: WE (A_s=5.59 cm^2), and 4 flat specimens (2@X65-0.05%C: A_s≈13 cm^2 each, 2@X65-0.13%C: A_s≈9 cm^2 each)
Solution volume to sample surface ratio, ml/cm^2	360	113
[H_2S], M	0.00385	
pH_2S, bar	0.08	0.18
pH @ operating conditions	4.0	
Duration	4 days	
Stirring speed	1000 rpm	
Measurement methods	Weight loss, LPR, EIS	
Surface characterization	XRD, SEM/EDS, Profilometry	

[‡] Trade name

After the solution in the autoclave was sparged with N_2 sparged for at least 2 hours and the temperature was increased to 50 °C, specimens were inserted in the autoclave, which was then closed and sealed by tightening bolts in a specific pattern; the autoclave was then pressurized above 8 bar with N_2 to check for leaks. During the leak check, the impeller was started (1000 rpm). After checking for leaks, the N_2 gas was released to a total pressure of about 1 bar. The system was then pressurized with an H_2S/N_2 mix to the calculated pressure, and a gas sample taken. Pressure was added to the autoclave in consideration of the desired total molar amount of H_2S needed. After that, the system was left for 30 minutes to 1 hour to stabilize, and then another gas sample is taken to check if the stabilized H_2S concentration in the gas phase matches the calculated value. If there is no need for further H_2S concentration adjustments, temperature was increased to 80 °C or 160 °C. The stable operating temperature was achieved within 2 hours. After this, the open circuit potential (OCP) was measured after reaching a stable value (+/- 0.1 mV/min). Linear polarization resistance (LPR) measurements were performed every 2 hours and electrochemical impedance spectroscopy (EIS) measurements every 24 hours during the next 4-day period. After the data collection was completed, the autoclave was cooled down for about 3 hours after the 80 °C experiments and 11 hours after the 160 °C experiments. When a temperature of 50 °C was achieved, the H_2S gas sample was taken, and the final pH of the bulk solution was measured. At the end of the test, pH is measured using the same pH probe in a specially made external probe holder which allows fluid from the autoclave to flow past the probe and into a controlled waste container with no loss of containment. The autoclave was then depressurized completely, purged with N_2 for one hour, and opened. Specimens were removed, rinsed with isopropanol, dried, and a 10 mL liquid sample was taken from the autoclave to measure the Fe^{2+} concentration using a calibrated UV-Vis spectrophotometric method. Based on the Fe^{2+} concentration and the assumption that any corrosion occurring during the temperature transition times had a negligible effect on the Fe^{2+} concentration, the expected pH values at tested temperatures were calculated using the concentration-based water chemistry model, incorporating the hydrogen sulfide dissociation constants described by Ma.[8]

RESULTS AND DISCUSSION

Corrosion rates at 80 and 160 °C

Figure 2 demonstrates the change in LPR corrosion rate with time, and repeatability of the experiments at the two temperatures tested. It is seen that the trend is similar for both temperatures, but the corrosion rate stabilized more quickly at 160 °C. The corrosion rates in both cases decreased with time due to the formation of a corrosion product layer. Each experiment was repeated twice. Error bars represent the maximum and minimum of corrosion rates at each period. Corrosion rates were calculated using B values of 15 mV/decade at 80 °C and 19 mV/decade at 160 °C. These B values were calculated using Equation (3):

$$B = \frac{\beta_a \beta_c}{2.3(\beta_a + \beta_c)} \tag{3}$$

where β_a and β_c are the anodic and cathodic Tafel slopes respectively. Their values can be found using Equations (4-5) described by Nesic, *et al*., for Fe dissolution and H^+ reduction reactions accordingly:

$$\beta_a = \frac{2.3RT}{1.5F} \tag{4}$$

$$\beta_c = \frac{2.3RT}{0.5F} \tag{5}$$

where R is gas constant, T is temperature, and F is Faraday constant.[9]

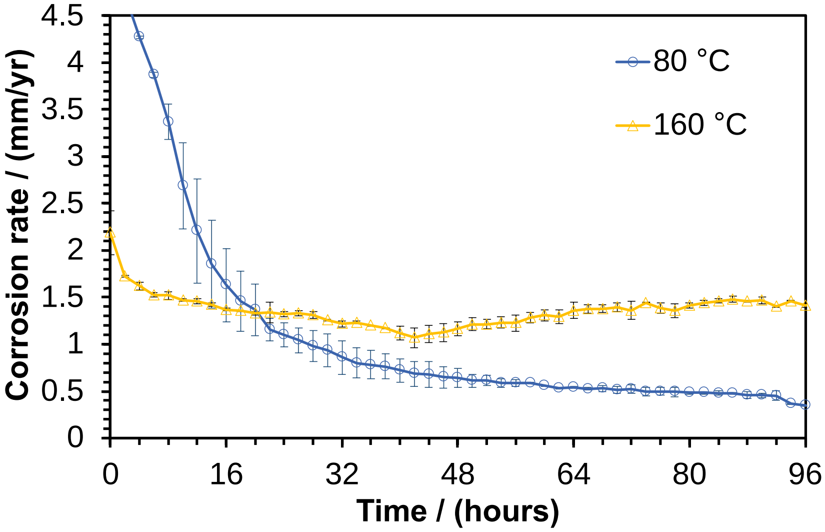

Figure 2. LPR corrosion rate with time at 80 °C and 160 °C

Figure 3 shows the comparison between integrated average LPR corrosion rate values and weight loss (WL) measurements. There was uncertainty in determining the appropriate B values for LPR corrosion rate calculations, particularly whether the cathodic reaction was governed by charge transfer or mass transfer processes. To resolve this, two sets of LPR corrosion rates were computed: one assuming charge transfer control, corresponding to the values presented in Figure 2, and another assuming mass transfer control. For the mass transfer-controlled scenario, Equation (4) was utilized again, but the cathodic Tafel slope was assumed to approach infinity, causing Equation (3) to transform into:

$$B = \frac{\beta_a}{2.3} \tag{6}$$

The B values calculated for this case were 20 mV/decade at 80 °C, and 25 mV/decade at 160 °C.

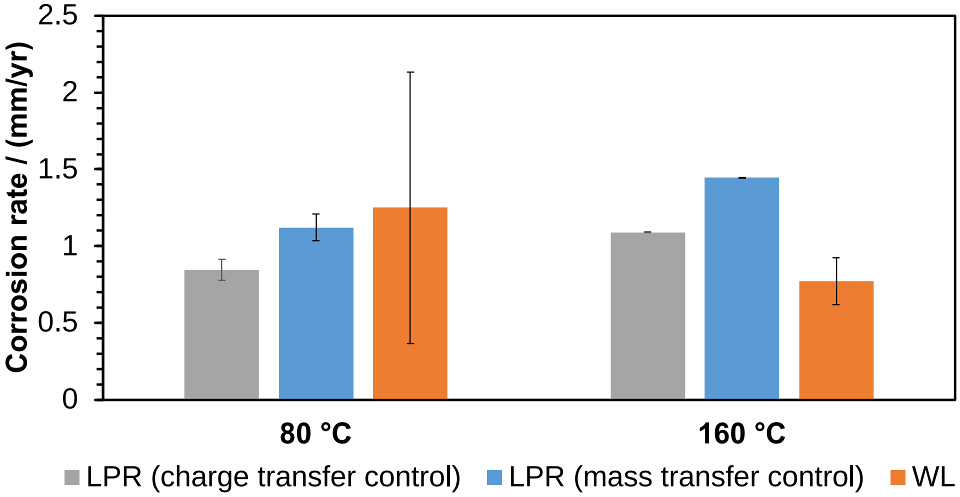

Figure 3. Comparison of corrosion rates over time at 80 °C and 160 °C, using integrated average LPR values calculated with B values assuming either charge transfer or mass transfer control, alongside WL measurements

For 80 °C, the values across all measurement types are quite similar, falling within the error bars of the WL measurements. However, the error bars for the WL results at 80 °C are much larger compared to those at 160 °C, representing the max/min of WL samples taken from different experiments. For 160 °C, the LPR values based on charge transfer closely match the WL results. Still, it is difficult to determine whether the corrosion process is controlled purely by charge or mass transfer; the actual results likely fall somewhere in between. The difference between WL corrosion rates at the two temperatures is statistically insignificant, as shown by the overlapping error bars.

A summary of experimental conditions and results is shown in Table 3. The targeted initial and final conditions were calculated from the measured conditions at 50 °C in the beginning and the end of the experiments. As can be seen, the calculated values of pH increased during the 4-day experiments from pH 4.0 to pH 4.89±0.34 and pH 5.09±0.16 for 80 °C and 160 °C respectively.

Table 3
Summary of experimentally measured and calculated results

	Initial measured conditions at 50 °C	Targeted initial conditions, calculated at T (°C) and pH 4.0	Calculated conditions at the end of the test time at target temperature based on Fe^{2+} measurements at 50 °C		Measured conditions at 50 °C, after cool-down procedures		
T (°C)	pH_2S (bar)	pH_2S (bar)	pH_2S (bar)	pH	pH_2S (bar)	pH	Fe^{2+} (ppm)
80	0.07	0.08	0.08±0.01	4.89±0.34	0.06±0.01	5.18±0.05	4.86±2.29
160	0.10	0.18	0.12±0.01	5.09±0.16	0.06	4.95±0.11	3.75±2.38

EIS analysis at 80 and 160 °C

EIS was run during experiments to better characterize processes occurring in the system. It is a very useful technique because, compared to DC methods limited by the slowest step, EIS can give information about several processes happening simultaneously in the system. However, interpretation of EIS data can be rather challenging, and there are still a lot of contradictions in the literature.

Figure 4 demonstrates the comparison between the EIS data obtained at 80 and 160 °C. At 80 °C, the EIS was conducted at the beginning and at the end of each 4-day experiment, while at 160 °C the measurements were taken daily at the same time. There is a big difference between the time constants at initial and final stages at 80 °C shown in Figure 4a. There are two time constants in both timeframes, however, a Warburg impedance can be observed at the end of the experiment meaning that the corrosion mechanism changed during the experiment.

For 160 °C, shown in Figure 4b, the overall trend for each day is the same; every measurement shows three time constants overlapping each other. The shape does not change during the 4-day period, meaning that the corrosion mechanism in the beginning of the measurements is the same as during and at the end of the test.

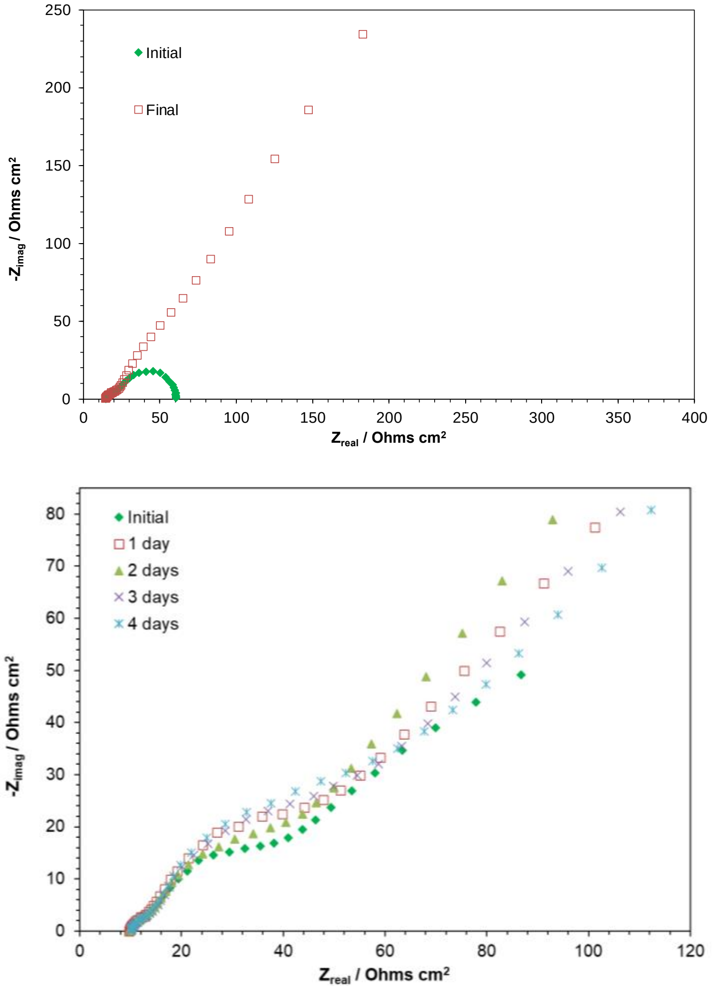

(a)

(b)

Figure 4. EIS analysis of samples exposed to H_2S environment for 4 days at: (a) 80 °C; (b) 160 °C

Surface Analysis at 80 and 160 °C

SEM images of corrosion product layers formed at 80 and 160 °C after 4 days of exposure are shown in Figure 5. For the sample at 80 °C, the crystals are locally concentrated and the polishing marks can be seen on the surface. This can be due to a thin corrosion product layer. Energy dispersive X-ray spectroscopy (EDS) analysis detects iron and sulfur both on the crystal and gap areas but indicates enhanced concentrations of residual alloying elements.

Figure 5b and c show that the corrosion product layers formed on different types of X65 with 0.05% C and 0.13% C are very similar. The rhombohedral type of crystals with similar size can be seen on both types of X65 steel. However, the corrosion product layer formed at 160 °C covers the surface of the metal much better, such that fewer polishing marks or gaps can be seen as in the case of 80 °C. EDS analysis indicates iron, sulfur, and other alloying elements (present on both types of steel as residues). Specimens required further analysis by XRD to establish phase identity.

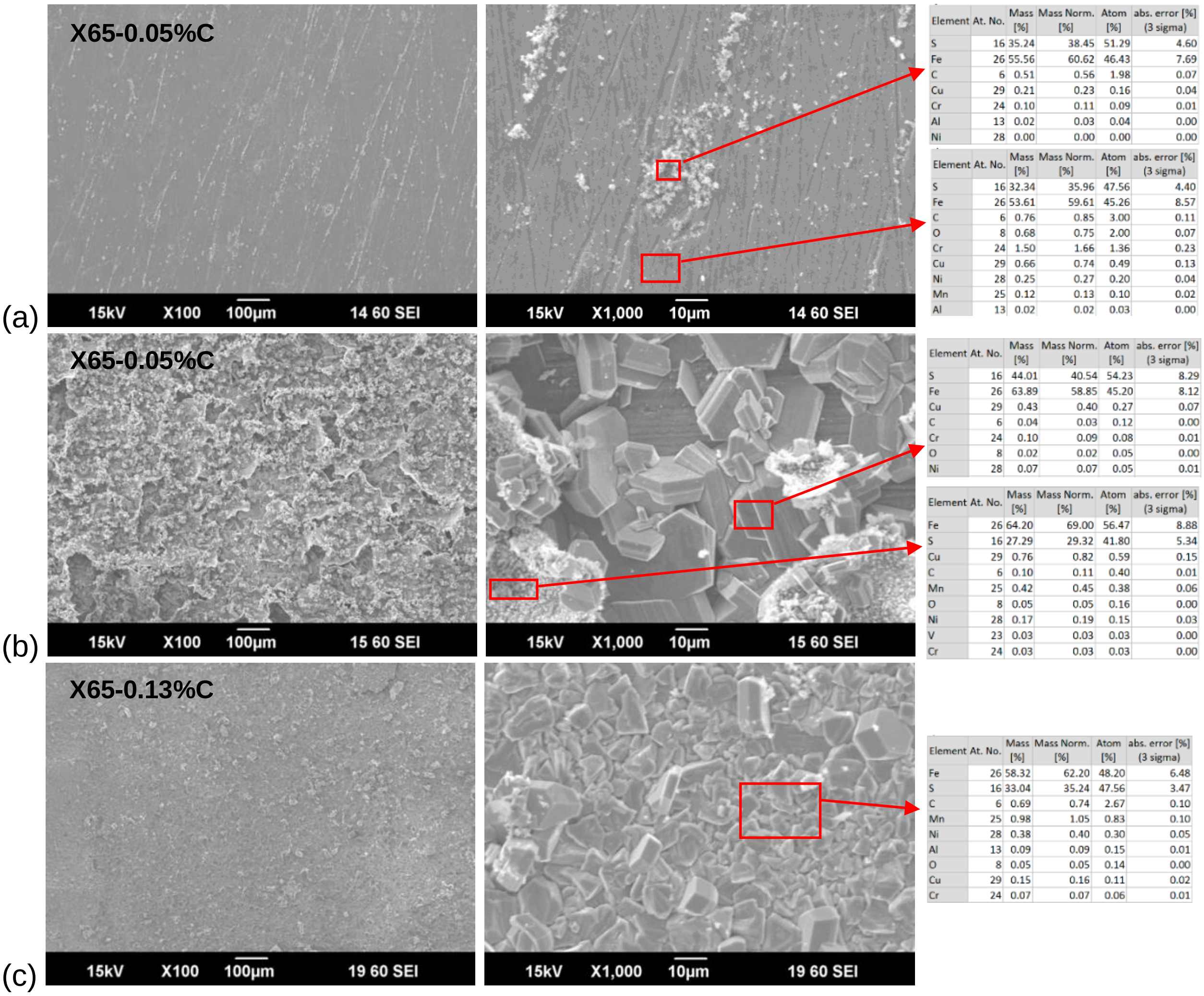

Element	At. No.	Mass [%]	Mass Norm. [%]	Atom [%]	abs. error [%] (3 sigma)
S	16	35.24	38.45	51.29	4.60
Fe	26	55.56	60.62	46.43	7.69
C	6	0.51	0.56	1.98	0.07
Cu	29	0.21	0.23	0.16	0.04
Cr	24	0.10	0.11	0.09	0.01
Al	13	0.02	0.03	0.04	0.00
Ni	28	0.00	0.00	0.00	0.00

Element	At. No.	Mass [%]	Mass Norm. [%]	Atom [%]	abs. error [%] (3 sigma)
S	16	32.34	35.96	47.56	4.40
Fe	26	53.61	59.61	45.26	8.57
C	6	0.76	0.85	3.00	0.11
O	8	0.68	0.75	2.00	0.07
Cr	24	1.50	1.66	1.36	0.23
Cu	29	0.66	0.74	0.49	0.13
Ni	28	0.25	0.27	0.20	0.04
Mn	25	0.12	0.13	0.10	0.02
Al	13	0.02	0.02	0.03	0.00

Element	At. No.	Mass [%]	Mass Norm. [%]	Atom [%]	abs. error [%] (3 sigma)
S	16	44.01	40.54	54.23	8.29
Fe	26	63.89	58.85	45.20	8.12
Cu	29	0.43	0.40	0.27	0.07
C	6	0.04	0.03	0.12	0.00
Cr	24	0.10	0.09	0.08	0.01
O	8	0.02	0.02	0.05	0.00
Ni	28	0.07	0.07	0.05	0.01

Element	At. No.	Mass [%]	Mass Norm. [%]	Atom [%]	abs. error [%] (3 sigma)
Fe	26	64.20	69.00	56.47	8.88
S	16	27.29	29.32	41.80	5.34
Cu	29	0.76	0.82	0.59	0.15
C	6	0.10	0.11	0.40	0.01
Mn	25	0.42	0.45	0.38	0.06
O	8	0.05	0.05	0.16	0.00
Ni	28	0.17	0.19	0.15	0.03
V	23	0.03	0.03	0.03	0.00
Cr	24	0.03	0.03	0.03	0.00

Element	At. No.	Mass [%]	Mass Norm. [%]	Atom [%]	abs. error [%] (3 sigma)
Fe	26	58.32	62.20	48.20	6.48
S	16	33.04	35.24	47.56	3.47
C	6	0.69	0.74	2.67	0.10
Mn	25	0.98	1.05	0.83	0.10
Ni	28	0.38	0.40	0.30	0.05
Al	13	0.09	0.09	0.15	0.01
O	8	0.05	0.05	0.14	0.00
Cu	29	0.15	0.16	0.11	0.02
Cr	24	0.07	0.07	0.06	0.01

Figure 5. SEM pictures of samples exposed to H_2S environment for 4 days at: (a) 80 °C; (b) and (c) 160 °C

XRD data in Figure 6a shows that the most intense peak is attributed to mackinawite, and the second highest to iron (α-Fe). The iron peaks could appear due to the mackinawite layer on the surface being thin, and X-rays penetrating through it. References for XRD peaks are listed in Appendix A.

The highest peak for the X65-0.13%C steel specimen in Figure 6b is attributed to iron, and the second highest to mackinawite. Also, there are several peaks matching with pyrrhotite, meaning that the predominant part of the corrosion product layer consists of pyrrhotite and mackinawite. Magnetite (Fe_3O_4) was observed in previous research[1] as an inner corrosion product layer between iron sulfides and the steel surface in an H_2S "only" environment. Magnetite may appear in the XRD results because the iron sulfide layer is thin enough for X-rays to penetrate it, which could also explain the presence of iron peaks. Lowest intensity peaks were attributed to pyrite and troilite.

Figure 6c combines XRD patterns for two different types of steel exposed to the same environment. As can be seen, the peaks are overlapping, meaning that the same corrosion product layers were formed on both types of X65 steel. In the case of X65-0.05%C, the most intense peak corresponds to mackinawite, followed by iron. The relative intensities of the two labelled α-Fe XRD peaks appear to be consistent. This could be likely due to the variability in the layer thickness which was observed in the SEM images in Figure 5b, which revealed gaps between the rhombohedral crystals. Similar to X65-0.13%C, pyrrhotite and magnetite are present on the surface of the steel, and possibly pyrite and troilite.

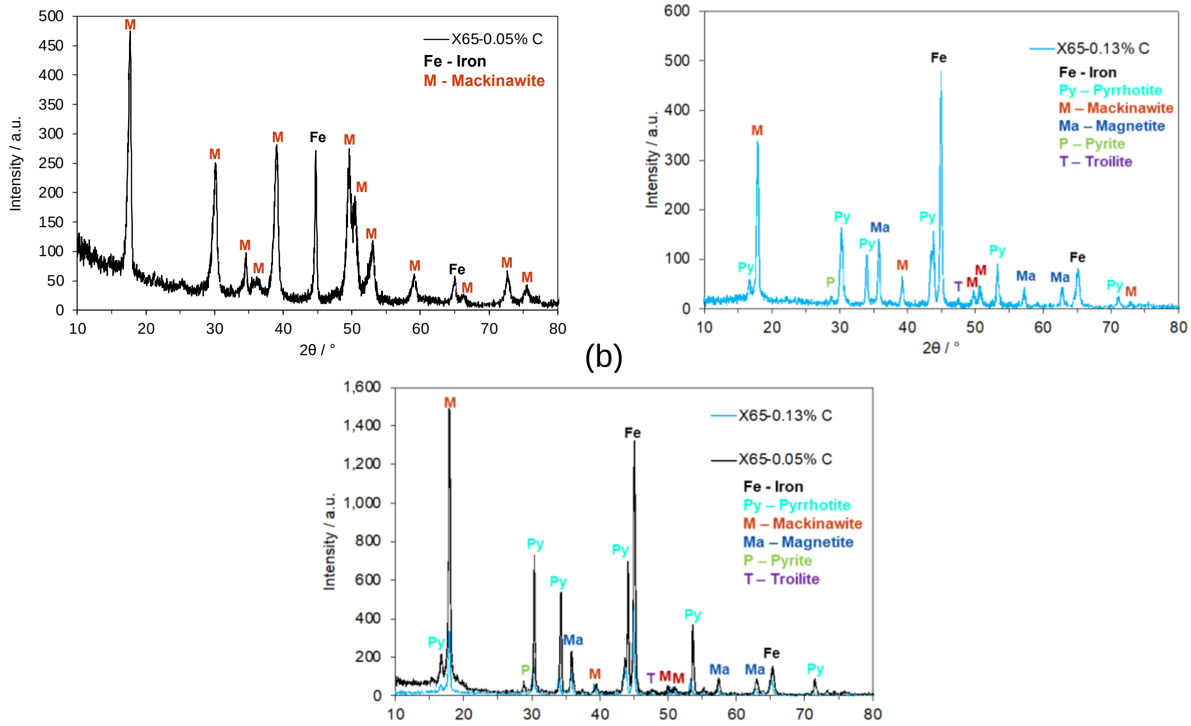

(a)

(b)

(c)

Figure 6. XRD analysis of the specimen exposed to H_2S environment for 4 days at: (a) 80 °C; (b) and (c) 160 °C

Profilometry analysis was conducted on the surface of each WL sample after removal of the corrosion product layer using a Clarke solution procedure[10] (Figure 7). To exclude edge effects, only the middle part of each sample was analyzed. The X65-0.05%C, tested at 80 °C, was found to have a surface roughness around ±2 µm and no localized corrosion was found. Similarly, the surface roughness of the X65-0.13%C specimen after 160 °C experiment was found to be approximately ±4 µm (Figure 7c) with no localized corrosion observed. One of the X65-0.05%C samples had localized corrosion with a maximum pit depth of 51 µm (Figure 7b). The calculated pitting ratio was 3.8, and penetration rate was found to be 4.4 mm/y. This demonstrates that pitting could occur in the tested conditions at 160 °C.

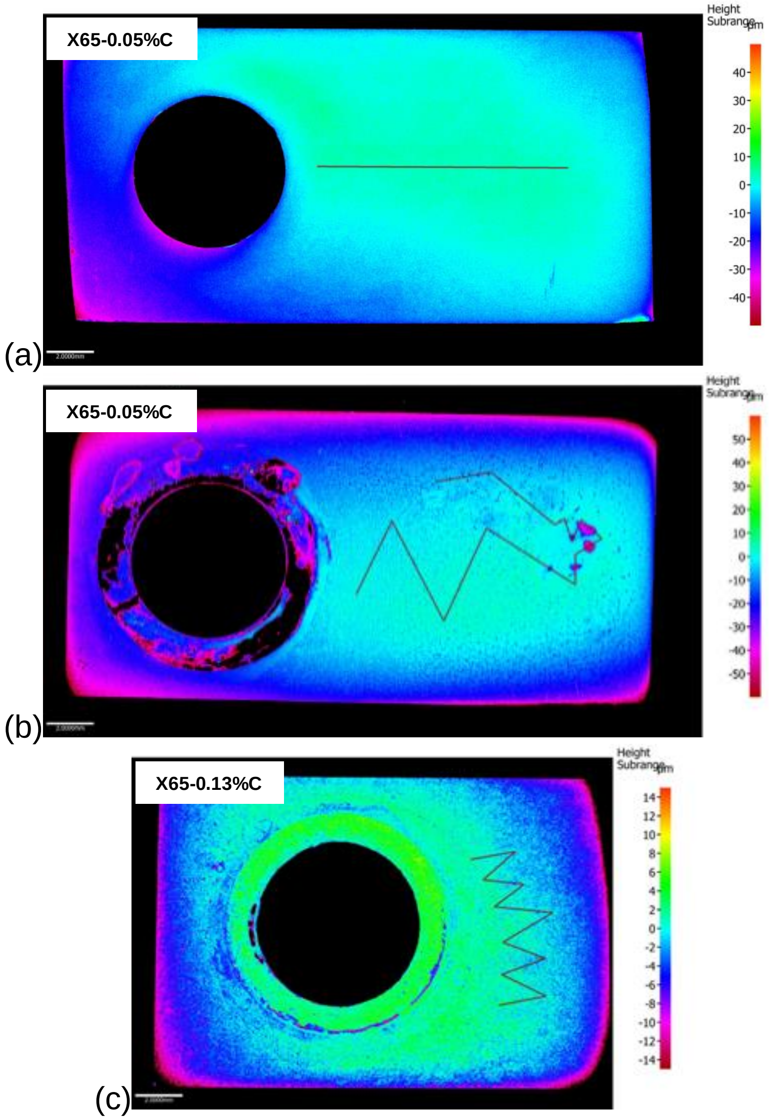

Figure 7. Profilometry analysis of the specimen exposed to H_2S environment for 4 days at: (a) 80 °C; (b) and (c) 160 °C

Cross-sectional analysis of samples was done for each of the experiments. The results for one of the repeats at 80 °C are shown in Figure 8a. As can be seen, the layer thickness varied between 5 to 12 µm and predominantly contained sulfides. The EDS line scan further supports previous findings, indicating sulfur and iron levels consistent with the formation of an iron sulfide layer. When the steel surface is reached, there is no sulfur present and iron content increases to a maximum.

Figure 8b and c demonstrate the corrosion product layers formed on X65-0.05%C and X65-0.13%C samples during 160 °C experiments; the thicknesses of the layers are similar (12 and 17 µm, respectively). Similar to 80 °C, the EDS mapping analysis demonstrated that the corrosion product layer on both types of steel consists mostly of iron and sulfur at the top of the layer. However, different from the experiments at 80 °C, iron and oxygen are present under the iron sulfide layer. These elements are an indication that magnetite was present under the iron sulfide layer, which was also confirmed using XRD.

There were some differences in thicknesses of corrosion product layers for X65-0.05%C and X65-0.13%C, where the magnetite layer thicknesses are 4 and 8 µm and iron sulfide layers are 12 and 11 µm in thickness, respectively.

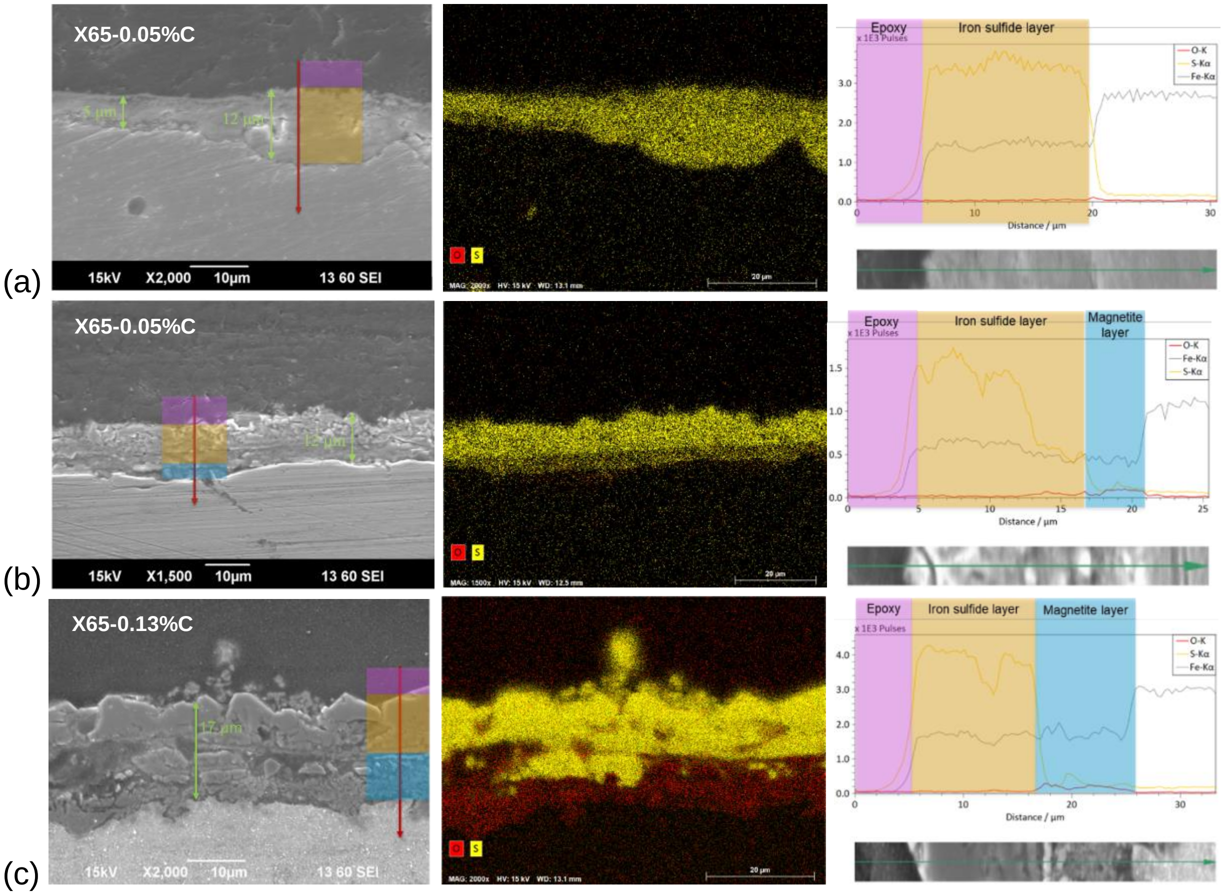

Figure 8. EDS mapping and line scan analysis of cross-section of the specimen exposed to H_2S environment for 4 days at: (a) 80 °C; (b) and (c) 160 °C

Comparison to literature results

The same conditions for H_2S experiments were used by Gao[1], so the comparison can be made between current and literature results. XRD analysis at 80 °C done by Gao[1] demonstrated that mackinawite was also the predominant corrosion product. At 160 °C as reported in the literature, the formed corrosion product layer consisted predominantly of pyrrhotite, whereas the current results observed the presence of a mackinawite and pyrrhotite combination with an inner magnetite layer. Gao's cross-sectional results[1] also show the presence of magnetite under iron sulfide at 160 °C, but this was not observed by XRD which is assumed to be due to a thick iron sulfide layer. Additionally, magnetite was observed at 80 °C in Gao's cross-sections, but it was not detected in the current experiments. This may be attributed to the formation of an extremely thin magnetite layer on the nanoscale level, which is difficult to detect by these analysis methods.

CONCLUSIONS

A repeatable procedure for working with H_2S at higher temperatures was developed and tested. Iron sulfide layers were formed both at 80 °C and 160 °C . Similar to previous research by Gao[1], mackinawite was formed at 80 °C, and pyrrhotite at 160 °C. However, the magnetite that Gao[1] observed both at 80 °C and 160 °C appeared only at 160 °C in the current experiments. Also, localized corrosion was found on the surface of one sample at 160 °C. The corrosion rate decreased with time for both temperatures as expected but remained relatively high due to corrosion product layers being unprotective.

ACKNOWLEDGEMENTS

The author would like to thank the following companies for their financial support: Ansys, Baker Hughes, ChampionX LLC, Chevron Energy Technology, Coastal Chemical Co., ConocoPhillips, ExxonMobil, SLB, Occidental Oil Company, Pertamina, Saudi Aramco, Shell Global Solutions and TotalEnergies.

REFERENCES

1. S. Gao, “Thermodynamics and Kinetics of Hydrogen Sulfide Corrosion of Mild Steel at Elevated Temperatures,” [Doctoral dissertation]. (Ohio University, 2018).
2. F. Pessu, Y. Hua, R. Barker, A. Neville, “A Study of the Pitting and Uniform Corrosion Characteristics of X65 Carbon Steel in Different H_2S-CO_2-Containing Environments,” Corrosion, 74, 8 (2018): pp. 886–902.
3. S. N. Smith, M. W. Joosten, “Corrosion of carbon steel by H_2S in CO_2 containing oilfield environments,” CORROSION 2006, paper no. 06115. (San Diego, CA: NACE, 2006)
4. D. W. Shoesmith, P. Taylor, M. G. Bailey, D. G. Owen, “The formation of ferrous monosulfide polymorphs during the corrosion of iron by aqueous hydrogen sulfide at 21 C,” Journal of the Electrochemical Society, 127, 5 (1980): pp. 1007.
5. P. Bai, H. Zhao, S. Zheng, C. Chen, “Initiation and developmental stages of steel corrosion in wet H_2S environments,” Corrosion Science, 93 (2015): pp. 109–119.
6. J. Ning, Y. Zheng, B. Brown, D. Young, S. Nešić, “A thermodynamic model for the prediction of mild steel corrosion products in an aqueous hydrogen sulfide environment,” Corrosion, 71, 8 (2015): pp. 945–960.
7. S. Gao, B. Brown, D. Young, S. Nesic, M. Singer, “Formation Mechanisms of Iron Oxide and Iron Sulfide at High Temperature in Aqueous H_2S Corrosion Environment,” Journal of The Electrochemical Society, 165, 3 (2018): pp. C171–C179.
8. Z. Ma, “Precipitation Kinetics of $FeCO_3$ and FeS on Steel Substrate,” [Doctoral dissertation]. (Ohio University, 2018).
9. S. Nesic, A. Kahyarian, Y. S. Choi, “Implementation of a comprehensive mechanistic prediction model of mild steel corrosion in multiphase oil and gas pipelines,” *Corrosion*, *75*, 3 (2019): 274-291.

10. ASTM G1-03, “Standard practice for preparing, cleaning, and evaluation corrosion test specimens,” (West Conschohocken, PA: ASTM).

APPENDIX A

A1. Lennie, A. R., Redfern, S. A., Schofield, P. F., & Vaughan, D. J. (1995). Synthesis and Rietveld crystal structure refinement of mackinawite, tetragonal FeS. *Mineralogical Magazine*, *59*(397), 677-683.
A2. Powell, A. V., Vaqueiro, P., Knight, K. S., Chapon, L. C., & Sánchez, R. D. (2004). Structure and magnetism in synthetic pyrrhotite Fe_7S_8: A powder neutron-diffraction study. *Physical Review B*, *70*(1), 014415.
A3. Ramsdell, L. S. (1925). The crystal structure of some metallic sulfides. *American Mineralogist: Journal of Earth and Planetary Materials*, *10*(9), 281-304.
A4. Skála, R., Císařová, I., & Drábek, M. (2006). Inversion twinning in troilite. *American Mineralogist*, *91*(5-6), 917-921.
A5. Iron Card No.: 01-071-4649
A6. Magnetite Card No.: 01-089-0691